Photoassociative formation of ultracold RbCs molecules in the (2) $^3\Pi$ state

Zhonghua Ji, Hongshan Zhang, Jizhou Wu, Jinpeng Yuan, Yonggang Yang, Yanting Zhao,* Jie Ma, Lirong Wang, Liantuan Xiao, and Suotang Jia

State Key Laboratory of Quantum Optics and Quantum Optics Devices, Laser Spectroscopy Laboratory, College of Physics and Electronic Engineering, Shanxi University, Taiyuan 030006, People's Republic of China

(Received 26 September 2011; published 3 January 2012)

We have investigated photoassociative formation of RbCs molecules in the (2) $^3\Pi$ excited state correlated to $v = 8$, $(5)0^+$ vibrational level in detail. The metastable ground-state RbCs molecules formed by spontaneous decay are ionized by pulsed dye laser through resonance-enhanced two-photon ionization. A rate equation of the photoionization process is introduced to explain the dependence of $RbCs^+$ molecular ion intensity on the ionization laser intensity. The saturation effect of molecular ion intensity appears as the photoassociation laser intensity increases. The rotational constant and centrifugal distortion constant are derived to be 0.01304 cm^{-1} and 0.000015 cm^{-1} from the photoassociation spectrum with a high sensitivity, respectively. The measured electric dipole moment of the observed (2) $^3\Pi$ state RbCs molecules is 4.7(6) D by Stark effect in static electric field.

DOI: 10.1103/PhysRevA.85.013401 PACS number(s): 37.10.Mn, 32.80.Rm, 33.15.Mt, 33.15.Kr

I. INTRODUCTION

Ultracold molecules provide novel possible applications in many areas of physics ranging from precision measurement to quantum computing [1]. Ultracold polar molecules are of particular interest because they interact strongly with applied electric fields for their permanent electric dipole moments (EDM) and the dipole-dipole intramolecular interactions are long-range, anisotropic, and tunable. With their complex internal structures, the potential applications of polar molecules include a novel quantum degenerate system [2], tests of fundamental symmetries [3], quantum chemistry [4], and quantum computation [5].

The methods of producing heteronuclear dimmers in sub-milli-Kelvin temperature contain mainly magnetically tunable Feshbach resonance [6] and light-assisted photoassociation (PA) [7]. To our knowledge, heteronuclear photoassociative molecules have been produced in LiCs [8], NaCs [9], KRb [10], RbCs [11], YbRb [12], and recently LiK [13], while Feshbach resonance has been applied to LiNa [14], LiK [15], LiRb [16], KRb [17], and RbCs [18]. A few specific species of other molecules are amenable to direct laser cooling to ultralow temperature [19]. Recently, a sympathetic cooling method was also considered for the LiH molecule [20].

It is very important to prepare a molecular sample in deeply bound levels of a singlet ground state because these rovibrational states are highly polarizable and stable. However, the molecules formed by either photoassociation or Feshbach resonance are typically in weakly bound levels, and it is necessary to transfer these unstable molecules to deeply bound levels. In the case of RbCs [11], the rovibrational ground state has been achieved using an incoherent stimulated emission pump-dump scheme from photoassociative molecules followed by spontaneous emission. For the case of KRb, an elegant, but more complex, coherent control technique, the two-photon stimulated Raman adiabatic passage (STIRAP) process, was used to produce the rovibrational singlet ground-state molecules starting from Feshbach resonance molecules [21,22] or photoassociative molecules [23]. In very limited cases, photoassociation may directly produce molecules in their rovibrational ground state only through spontaneous emission, such as in the case of LiCs [8].

The RbCs molecule is of particular interest for many reasons. It has a large Frank-Condon (FC) factor [24] and is a candidate to serve as a qubit in quantum information processing. A crucial benefit of RbCs molecules is that they are stable against an atom exchange reaction of the form $RbCs + RbCs \rightarrow Rb_2 + Cs_2$ in the rovibrational ground state, unlike the KRb molecule [25]. In addition, a Bose-Einstein condensate (BEC) has been successfully obtained for both atomic species [26,27], and experiments with dense ultracold ensembles of both species have also been realized [28,29]. Since RbCs molecules are bosons, such a system could be exploited for a BEC of polar molecules. In addition to the mentioned stimulated emission pump-dump scheme [11], some other promising pathways to produce stable lowest rovibrational RbCs molecules are also proposed and implemented. Just as in the case of KRb [21,22], a similar STIRAP scheme is also used to produce rovibrational ground-state RbCs molecules with high phase-space density in Innsbruck [30,31] and Durham [32]. The methods of resonance coupling, either (1) $^1\Pi \sim$ (2) $^1\Pi$ [33] or $A\,^1\Sigma^+ \sim b\,^3\Pi$ [34], are explored to the formation of RbCs molecules in the lowest rovibrational ground state. Recently, Gabbanini *et al.* [35] observed metastable triplet ground-state RbCs molecules produced by photoassociation followed by radiative stabilization. These levels are at short range, implying the possibility of direct photoassociation to the lowest levels of the $X\,^1\Sigma^+$ with spin-orbit coupling between the (2) $^3\Pi$ and (2) $^1\Pi$ states. The simplicity of this single PA step has drawn our attention because it displays an attractive technique to produce the lowest level of RbCs molecules, very similar to LiCs [8].

In this paper, we investigate photoassociative formation of RbCs molecules in the (2) $^3\Pi$ state with a high sensitivity. We extract the corresponding rotational constant and centrifugal distortion constant based on a nonrigid model from the

*Corresponding author: zhaoyt@sxu.edu.cn

measured photoassociation spectrum and assign the observed short-range molecular state. We study the dependence of $RbCs^+$ molecular ion intensity on the ionization laser intensity and PA laser intensity and explain our measurements with related theories. We also measure the electric dipole moment (EDM) of this short-range RbCs molecule by the dc Stark effect in a static electric field.

II. EXPERIMENT

Figure 1 shows the formation and ionization scheme of photoassociative RbCs molecules in the $(2)\,^3\Pi$ state. The potential energy curves (PECs) of RbCs molecules are based on the data in Refs. [36,37] and labeled with Hund case (a). The PA laser excites a pair of colliding ^{85}Rb and ^{133}Cs atoms into a deeply bound level at short range, which is the $(2)\,^3\Pi$ state correlated to the $Rb(5P_{1/2}) + Cs(6S_{1/2})$ atomic asymptote. Metastable molecules are formed from these excited molecules followed by spontaneous decay. They are then ionized by resonance-enhanced two-photon ionization (RETPI) through some intermediate states, such as the $(3)\,^3\Pi$ intermediate state correlated to the $Rb(5S_{1/2}) + Cs(5D_{3/2,5/2})$ atomic asymptote, and detected by a microchannel plate (MCP) using a time-of-flight (TOF) mass spectrometer. This ionization

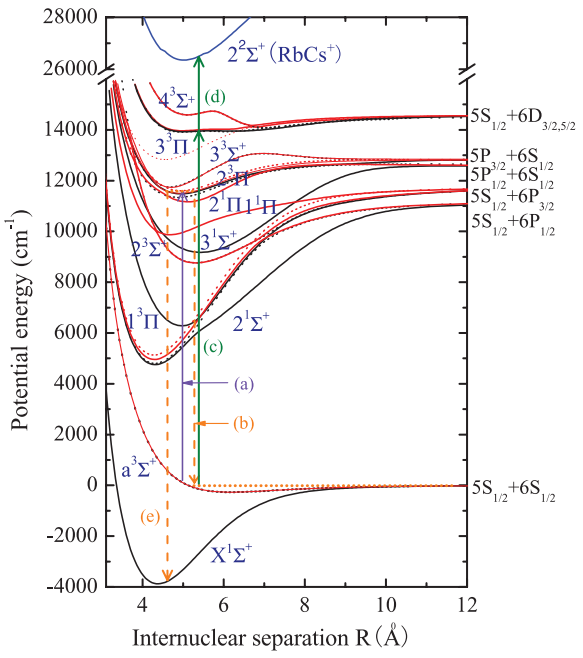

FIG. 1. (Color online) Formation and ionization scheme of RbCs molecules in the $(2)\,^3\Pi$ state. A pair of ^{85}Rb and ^{133}Cs atoms during collision is excited to a deeply bound level (a), which is the $(2)\,^3\Pi$ state correlated to the $Rb(5P_{1/2}) + Cs(6S_{1/2})$ atomic asymptote under a photoassociative photon. The metastable $a\,^3\Sigma^+$ state molecules are formed by spontaneous decay (b) and are ionized by resonance-enhanced two-photon ionization [(c) and (d)] through the $(3)\,^3\Pi$ intermediate state correlated to the $Rb(5S_{1/2}) + Cs(5D_{3/2,5/2})$ atomic asymptote. It is also likely that some of the excited-state molecules decay to the lowest level of the $X\,^1\Sigma^+$ ground state due to spin-orbit coupling between the $(2)\,^1\Pi$ and $(2)\,^3\Pi$ states (e). The potential energy curves of RbCs molecules are based on the data in Refs. [36,37] and labeled with Hund case (a).

scheme was also recently used to detect photoassociative RbCs molecules in a weakly bound 0^- state below the $Rb(5S_{1/2}) + Cs(P_{1/2})$ dissociation limit, from which only triplet ground-state RbCs molecules are populated because of the selection rule [38]. For more deeply bound vibrational levels associated with shorter internuclear distances, Hund case (a) is a better coupling description since the nuclear axial electric field is stronger. Considering the selection rules for transitions between molecules states in Hund case (a), there is probability to produce the lowest levels of $X\,^1\Sigma^+$ molecules from the single state $(2)\,^1\Pi$ due to the spin-orbit coupling with $(2)\,^3\Pi$. This is similar to the case of LiCs [8] with spin-orbit mixing of the $(1)\,^1\Pi$ state with triplet states [39]. The molecular number population in these two ground states is determined by FC factors between the initial- and final-state wave functions.

As the free-bound FC factor of photoassociation for heteronuclear molecules is significantly smaller than that for homonuclear molecules, our experiment operates in a dual-species, dark spontaneous force optical trap (dark SPOT) with a high atomic density [40] and a low collision rate [41]. We have vapor dispensers and an effusive oven for both Rb and Cs atoms in a stainless-steel chamber with a pressure of about 6.4×10^{-7} Pa. A pair of coils with anti-Helmholtz configuration generates about 15-G/cm magnetic gradient, and three other pairs of coils are placed around the vacuum chamber to compensate geomagnetism at the position of cold atom clouds. Four Littrow external-cavity diode lasers (DL100, Toptica) locked by saturation-absorption spectroscopy provide trapping and repumping beams for the two dark SPOTs. Two acousto-optic modulators (AOMs) are used to adjust Rb and Cs trapping laser frequencies, which are tuned to 12.5 and 15 MHz below the $5S_{1/2}(F = 3) \rightarrow 5P_{3/2}(F' = 4)$ cycling transition and the $6S_{1/2}(F = 4) \rightarrow 6P_{3/2}(F' = 5)$ transition, respectively. The powers of trapping beams for Rb and Cs are 30 and 50 mW. The frequencies of repumping beams for Rb and Cs atoms are turned to $5S_{1/2}(F = 2) \rightarrow 5P_{3/2}(F' = 3)$ and $6S_{1/2}(F = 3) \rightarrow 6P_{3/2}(F' = 4)$, respectively. The Rb and Cs repumping beam powers are both about 2 mW and are combined together by polarizing beam splitter (PBS) and half-wave plate ($\lambda/2$). The trapping and repumping beams are expanded to about 15 mm in diameter. The Rb and Cs depumping beams are generated from the Rb and Cs trapping lasers by two AOMs and tuned to the $5S_{1/2}(F = 3) \rightarrow 5P_{3/2}(F' = 2)$ transition and the $6S_{1/2}(F = 4) \rightarrow 6P_{3/2}(F' = 4)$ transition, respectively. The depumping beams for both Rb and Cs atoms with power of about 40 W and 3 mm in diameter are combined together with another PBS and $\lambda/2$. A black dot of 5 mm in diameter is placed in the center of the combined repumping beams while the combined Rb and Cs depumping beams fill the dark region in order to produce the Rb and Cs atoms in the lowest hyperfine states ($F = 2$ for Rb atoms and $F = 3$ for Cs atoms). In order to eliminate the Fresnel diffraction, the repumping and depumping beams of Rb and Cs atoms combined by another PBS and $\lambda/2$ pass through a pair of lenses ($f = 20$ cm) into the vacuum chamber. To characterize how dark the trap is, Ketterle *et al.* [42] used the parameter p to denote the fraction of atoms in the bright ground state and dark ground sate: $p = N_b/(N_b + N_d)$, where N_b and N_d represent the atomic numbers in bright and dark states, respectively. For example, N_b and N_d represent atomic numbers in $F = 4$ and $F = 3$

hyperfine ground states for the Cs dark SPOT. We measure the fraction p by adding a fill-in beam [40] whose frequency is the same as the repumping beam. The fluorescence intensity in the dark SPOT increases for $P1$ to $P2$ when the dumping beam is turned off and the fill-in beam is turned on. Thus, p is calculated by $p = P1/P2$. Townsend *et al.* [40] have studied the dependence of cold atomic density on the fraction p. They found that the density is largest when p is about 10%. In our experiment, the fraction increases from less than 10% to about 20% after optimization of the overlapped two atomic clouds. In addition, the optical path in our experiment is compact [38], and the diffuse reflection of repumping beams through one pair of the smallest windows of our stainless-steel chamber (MCF800-ExtOct-G2C8A16, Kimball Physics) also reduces the efficiency of two-species dark SPOTs.

Two charge-coupled-device (CCD) cameras, placed along the horizontal and vertical directions to verify good spatial overlap of two atom clouds, are used to measure each species dimension. The two atom clouds usually overlap about 80% in a diameter of less than 500 μm. With the best configuration, we can trap 2×10^8 rubidium atoms and 3×10^8 cesium atoms at densities of 3×10^{11} and 6×10^{11} cm^{-3}, respectively. The temperatures of Rb and Cs atom clouds are measured to be about 150 and 100 μK separately by time-of-flight absorption imaging.

The photoassociation laser is provided by a continuous-wave tunable Ti:sapphire laser system (MBR110, Coherent) with a typical linewidth of less than 100 kHz and output power up to ~600 mW. The frequency is monitored by a commercial wavelength meter (WS/7R, HighFinesse-Angstrom) with an absolute accuracy of 0.002 cm^{-1} (~60 MHz), which is calibrated by a stabilized He-Ne laser (SL-02, SIOS) or Cs atomic transition line. Additionally, we monitor Ti:sapphire frequency scan with a reference cavity, which is stabilized via the locked Cs repumping laser. This monitor system results in a relative accuracy of 3 MHz. The photoassociation laser is focused to the center of the overlapped cesium and rubidium dark SPOTs by optimizing the depletion of trapped cesium atoms with resonant frequency. The diameter of the PA beam is about 500 μm, resulting in available intensity up to ~300 W/cm^2.

We use two methods to measure the photoassociation process. The first method is trap loss, which is an indirect method for monitoring the photoassociative molecules: we measure the fluorescence of Rb and Cs cold atoms by a Si-Avalanche photodiode (APD-1.5, Licel), and the fluorescence variations indicate the trap loss induced by formation and dissociation of photoassociative molecules. The second method is photoionization, which is a direct method of monitoring photoassociative molecules: the ground-state RbCs molecules are ionized by RETPI and directly detected by the TOF mass spectrometer. In this paper, we focus on the second sensitive ionization detection method. The ionization laser in our experiment is provided by a pulsed dye laser (CBR-G-18EG, Spectra Physics) pumped by 532-nm Nd:YAG laser (INDI-40-10-HG, Spectra Physics) at a rate of 10 Hz. The pulsed laser can cover 680–760 nm with 8-ns duration using a Pyridine 2 dye molecule and is focused to the size of atoms with a lens.

Two external delay and pulse generators (DG535, Stanford-Research system) provide the master clock and control the timing of the trapping lasers, PA laser, and pulsed dye laser.

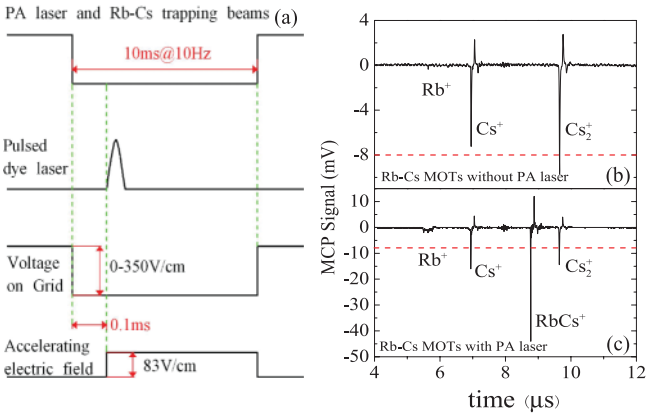

FIG. 2. (Color online) Experimental time sequence and typical time-of-flight mass spectrums. (a) Experimental time sequence (not to scale) in our experiment. An accelerating electric field is used to accelerate the ions ionized by the dye laser. Static electric field on the grid is used to measure the electric dipole moment of RbCs molecules by the dc Stark effect. (b) and (c) Ion signals detected by MCP in the absence and the presence of the PA laser. When the PA laser is focused on the Rb-Cs dark SPOTs, not only does the $RbCs^+$ molecular ion appear, but also the other ions are enhanced. The red dashed lines indicate the value of −8 mV on the vertical axis for comparison between (b) and (c).

Figure 2(a) shows the time sequence of our experiment. In order to suppress the Cs^+ atomic ion signal and ensure the produced RbCs molecules in the ground electronic state, the PA laser and trapping lasers for both Rb and Cs atoms are usually extinguished 100 μs before each ionization, such that the atoms mainly stay at ground state and there are few excited molecules. Thus, the atomic ion signals are strongly suppressed, and the effect on the $RbCs^+$ molecular ion signal is depressed because the ionization mechanisms for the Rb atom and Cs atom in the ground state are three-photon ionization [43] and two-photon ionization [44], respectively. The photoionized ions are then accelerated by an accelerating electric field (83 V/cm) and detected by a MCP. We then amplify the signals, monitor them on an oscilloscope, and record the signals using a NI PCI1714 card with a boxcar integrator (SRS-250, Stanford-Research system). In order to measure the EDM of these excited RbCs molecules using the dc Stark spectrum, different static electric-field strengths between 0 and 330 V/cm are applied to the atomic sample by two square electrodes with a side length of 36 mm and a distance of 48.1 mm. The electrodes have a central hole (Ø25 mm) for extraction of the ions produced; this pair of electrodes is also a part of the mass spectrometer used for the detection of the ground-state molecules, and the electric field on the electrodes is switched off 0.1 ms before the constant accelerating electric field.

We fix the PA laser at resonant frequency and can observe the RbCs molecular ion signal when the dye laser wavelength is in these ranges: 680–694, 700–717, and 740–745 nm, corresponding to ionization intermediate sates of $(4)\,^3\Sigma^+$, $(3)\,^3\Pi$, and $(3)\,^3\Sigma^+$. The $(3)\,^3\Sigma^+$ state is another intermediate state of RETPI for RbCs molecules [11,35]. In our experiment, we found that the atomic ion intensity has a great impact on the molecular ion intensity in the

range of 696–699 nm for the large detection efficiency for Rb^+ and Cs^+ atomic ions. As the $RbCs^+$ molecular ion intensity in the range 700–717 nm is larger than that in the other two ranges, we set the dye laser wavelength at about 710 nm.

Figures 2(b) and 2(c) show two typical time-of-fight spectrums detected by MCP as a function of time after the photoionization laser pulse in the absence and presence of the PA laser set at 120 W/cm^2, respectively. The pulsed dye laser energy is 1.5 mJ and is focused onto the trap with a waist of the order of 1 mm, resulting in 2.4×10^7 W/cm^2. The time interval between the ionizing laser pulse and the PA laser switching off is 100 μs. Because the detection efficiencies for the Cs atom and Cs_2 molecule are higher than those for the Rb atom and Rb_2 molecule at this dye laser wavelength [43,45], no Rb_2^+ molecular ion signal is observed, and the intensity of the Cs^+ atomic ion is much larger than that of the Rb^+ atomic ion.

We notice that the Cs_2^+ molecular ion signal appears even without Ti:sapphire laser, which is because the Cs trapping laser acts as a PA laser [Fig. 2(b)]. But we do not observe the $RbCs^+$ molecular ion in the absence of the Ti:sapphire PA laser. When the Ti:sapphire laser is tuned to the resonant frequency of RbCs molecules, not only does the $RbCs^+$ molecular ion appear, but also the Rb^+ and Cs^+ atomic ions and Cs_2^+ molecular ion are enhanced [Fig. 2(c)]. We mark two dashed lines at the same value of the vertical axis for comparison. This implies that in addition to the ionization of ground-state RbCs molecules, these following processes also take place when the ionization laser is applied:

$$RbCs + h\nu \rightarrow Rb^+ + Cs + e^-, \quad (1)$$

$$RbCs + h\nu \rightarrow Rb + Cs^+ + e^-. \quad (2)$$

As the Ti:sapphire laser is near the $6S_{1/2} + 6P_{3/2}$ atomic limit and the ground-state RbCs molecule is stable [25], the enhancement of the Cs_2^+ molecular ion is supposed to arise from the photoassociation of Cs atoms. The arrival times of Rb^+, Cs^+, $RbCs^+$, and Cs_2^+ are 5.64, 6.95, 8.77, and 9.65 μs when the PA laser is turned to resonant frequency, which agree with expected positions. We use a boxcar to record only negative voltage in order to avoid the impact from the oscillation that arises from the amplifier circuit.

The number of observed molecular ions is typically 100 per pulse, which is extracted from the characteristic time and amplitude of a single molecular ion detected by the MCP. The RbCs molecular production rate in the metastable ground state, which contains different rovibrational levels, is estimated to be 2.5×10^4 s^{-1} with the 10-Hz repetition frequency of the pulsed laser and a total efficiency of about ~4%, including the efficiencies of the ionization process and the detection process.

III. RESULTS AND DISCUSSION

A. Photoassociative spectrum of RbCs molecules in the (2) $^3\Pi$ state

Figure 3(a) shows the rotational structures of photoassociative RbCs molecules in the (2) $^3\Pi$ state. We observe totally five rotational levels with a high sensitivity, corresponding to $J = 0, 1, 2, 3$, and 4, whereas Gabbanini *et al.* [35] observed three rotational levels with low sensitivity. The signal-to-noise radio

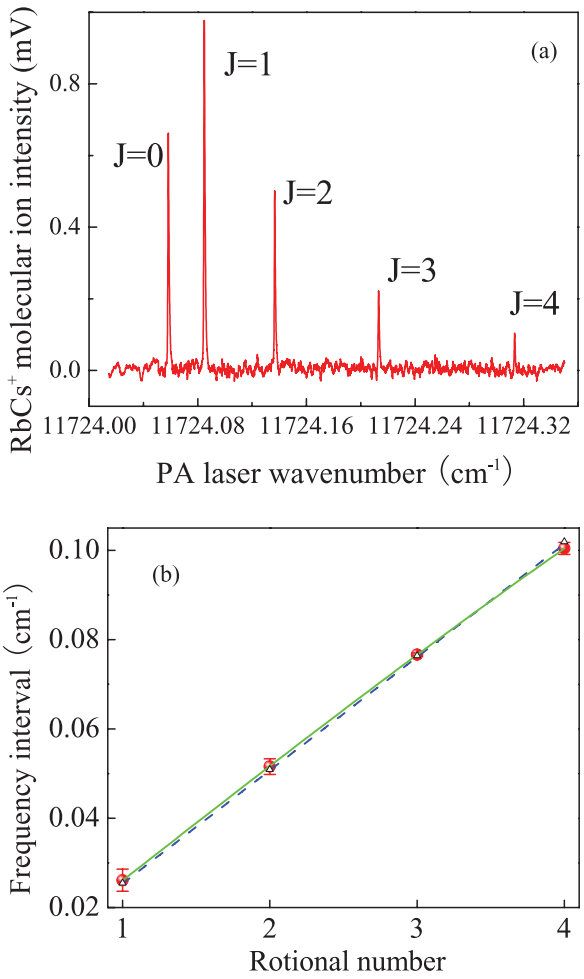

FIG. 3. (Color online) Photoassociative spectrum of RbCs molecules in the (2) $^3\Pi$ state and theoretical fit for the corresponding rotational constant and centrifugal distortion constant. (a) Rotational structures of photoassociative RbCs molecules in the (2) $^3\Pi$ state. The five peaks correspond to $J = 0$, 1, 2, 3, and 4 rotational levels of excited-state RbCs molecules at short range. (b) Dependence of the energy interval ΔE on the rotational number J for the (2) $^3\Pi$-state RbCs molecules. The red dots represent experimental data, and the error bars are the standard deviations derived from five different measurements. The blue dashed line and green solid line are fitted to Eq. (4) without and with centrifugal distortion constant D_v for the same experimental data. The square of coefficients of correlation R^2 in the two fit processes are 0.99914 and 0.99999, respectively.

(SNR) can reach up to about 20 for the rotational number $J = 1$ level in our experiment. The different intensities between rotational levels arise from FC factors for the photoassociation transitions between the initial state of two cold free atoms and the final rovibrational levels. The $J = 0$ resonance frequency of this state is 11724.058 cm^{-1} with absolute accuracy of 0.002 cm^{-1}, which is detuned to -8.076 cm^{-1} detuning relative to the $6S_{1/2} \rightarrow 6P_{3/2}$ transition of Cs at 11732.1342 cm^{-1}.

The highly sensitive rotational spectrum provides us with the opportunity to study the molecular constants for this short-range state with good precision. As the interaction between two constituent atoms of the excited molecule formed by photoassociation is weak compared to the ordinary chemical

bond, the nonrigid model can be used [46]. The rotation-vibration energy of a diatomic molecule is written as

$$E/hc = B_v J(J+1) - D_v J^2(J+1)^2 \quad (J \geqslant 0), \qquad (3)$$

where E is the rotational eigenvalue, h is the Planck constant, c is the speed of light, B_v is the rotational constant of the v vibrational state, D_v is the corresponding centrifugal distortion constant, and J is the rotational quantum number. Usually, D_v is typically several orders of magnitude smaller than B_v.

For the same vibrational quantum number, the energy interval ΔE of the neighboring rotational levels is

$$\begin{aligned}\Delta E &= [E(J) - E(J-1)]/hc \\ &= 2B_v J - 4D_v J^3 \quad (J \geqslant 1).\end{aligned} \qquad (4)$$

Figure 3(b) shows the dependence of the energy interval ΔE on the rotational number J for these excited-state RbCs molecules. The error bars are the standard deviations derived from five different measurements. The rotational constant B_v and centrifugal distortion constant D_v are derived to be 0.01304 and 0.000015 cm^{-1} by fitting experiment data with Eq. (4) [the green solid line in Fig. 3(b)]. The rotational constant B_v is also extracted by fitting the same experimental data with Eq. (4), but without centrifugal distortion constant D_v. This gives us the rotational constant B_v of 0.01268 cm^{-1} [the blue dashed line in Fig. 3(b)]. The errors of rotational constant in the two fit processes are 0.000027 and 0.000086 cm^{-1}, respectively. The square of coefficients of correlation R^2 are 0.99999 and 0.99914 in the two fit processes, respectively. From the fit errors, coefficients of correlation, and fit curves for these two fit processes, we conclude that it is still reasonable to use the nonrigid model for ultracold photoassociative molecules at short range. Including all other errors, such as errors from the determination of the resonant line position using Lorentz fit, standard deviations of level interval, reference cavity stability, and even photoassociation laser linear scanning, the total error of rotational constant B_v is less than 0.0004 cm^{-1}. The observed structure has no molecular hyperfine splitting and thus is assigned to one of the two $(5)0^+$ and $(4)0^-$ states, which have no angular momentum to couple with nuclear spins. We calculate all the rovibrational levels of the $(2)\,^3\Pi$ state based on the RbCs molecular PEC of Ref. [37], and the relative differences between the experimental and theoretical values are compared for these two states. Considering standard deviations near the observed state, the vibrational level for $v = 8$, $(5)0^+$ is best fitted with standard deviation 0.00086 cm^{-1}. We show the calculated energy intervals of this vibrational level with open triangles in Fig. 3(b). The calculated rotational constant for the $v = 8$, $(5)0^+$ level is 0.0127 cm^{-1}, which is consistent with the measured value within the error range. The $J = 0$ rational level frequencies of vibrational levels from 0 to 7 are calculated to be about -238.22, -207.63, -177.20, -147.01, -117.11, -87.40, -57.95, and -28.80 cm^{-1}, relative to the $v = 8$ vibrational level.

B. The dependence of $RbCs^+$ molecular ion intensity on ionization laser intensity and photoassociation laser intensity

We measure the dependence of $RbCs^+$ molecular ion signal intensity on the ionization laser intensity and photoassociation laser intensity as they effect the formation and detection of the photoassociative RbCs molecules.

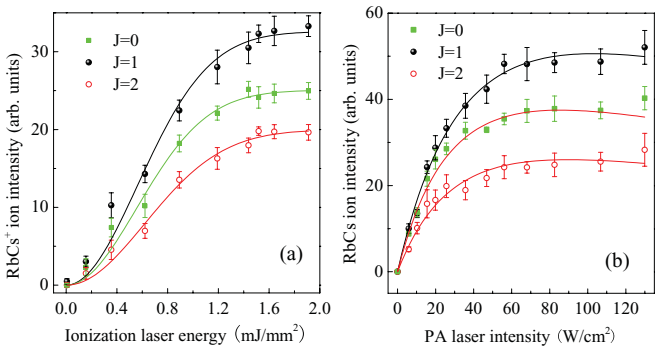

FIG. 4. (Color online) $RbCs^+$ molecular ion intensity for $J = 0$, 1, and 2 rotational levels as a function of ionization laser intensity (a) and PA laser intensity (b). The different lines in (a) are fitted to experimental data by Eq. (6). The lines show that a saturation effect appears when the pulsed ionization laser intensity is large enough. The curves in (b) represent the fits to the saturation model by Bohn and Julience, described in Eq. (8). The saturation intensities for $J = 0$, 1, and 2 are about 84, 102, and 93 W/cm^2, respectively.

Figure 4(a) shows the measured $RbCs^+$ molecular ion intensity for the $J = 0$, 1, and 2 rotational states of the $(2)\,^3\Pi$ state when the pulsed dye laser intensity varies from 0.15 to 1.91 mJ/mm^2 while PA laser power is fixed at about 200 mW.

We describe the two-photon photoionization process of ground-state RbCs molecules by this formula [47]:

$$dN_e/dt = (N_0 - N_e)\sigma^{(2)} I(t)^2, \qquad (5)$$

where $\sigma^{(2)}$ is the ionization coefficient for the two-photon ionization process, N_e is the number density of electrons and corresponds to the molecular ion intensity, and N_0 is the initial number density of neutral RbCs molecules. $I(t)$ is the peak intensity of pulsed laser. The pulsed laser is approximately modeled to be a square pulse; then $I(t)$ can be written as a constant $I(t) = I_0 = W/\tau_p A$, where W and τ_p are pulsed laser energy and width and A represents the beam area of the focal region. W/A is defined as pulsed laser intensity. We consider the time as a constant and pulsed laser energy as a variable; thus Eq. (5) can be solved:

$$N_e = N_0\left(1 - e^{-(\sigma^{(2)} W^2/\tau_p A^2)}\right). \qquad (6)$$

We fit the experimental data in Fig. 4(a) with this equation and extract the ionization coefficient to be about 0.07(3), which is consistent with what we mentioned in the experiment part. The error mainly comes from the focus region of the pulsed laser. The experiment data and theoretical fit agree well when the ionization laser intensity is large.

When the pulsed laser energy is low, Taylor expansion for Eq. (6) at $W = 0$ gives

$$N_e = 2\sigma^{(2)} N_0 W^2/A^2\tau_p. \qquad (7)$$

Equation (7) indicates that the photoionized molecular ion intensity should be dependent on the square of the dye laser intensity, as expected from the two-photon one-color transition from the ground-state molecules. This relationship has clearly

been observed in other experiments, such as Rb_2^+ [48] and KRb^+ [49].

The molecular ion intensity seems to be linear when the ionization laser intensity is low. We have observed a similar relationship between $Cs_2{}^+$ molecular ion intensity and ionization laser intensity but do not show it here because it is outside the subject of this paper. In fact, Drag *et al.* [50] also observed linear dependence of $Cs_2{}^+$ molecular ion intensity on dye laser intensity but did not observe the saturation effect in their experiment. The similar dependence of the molecular ion intensity arises from the same intermediate correlated atomic state of Cs ($5D_{3/2,5/2}$) in a window of about 700 cm^{-1} width, centered at 14 000 cm^{-1} [50]. This intermediate atomic state makes the transition from ground state to excited state more likely to saturate than the transition from excited state to ionic state [51], resulting in linear dependence.

We investigate the effect of the photoassociation laser intensity on $RbCs^+$ molecular ion intensity. Figure 4(b) shows the $RbCs^+$ molecular ion intensity for $J = 0, 1, 2$ rotational states of the (2) $^3\Pi$ state as a function of photoassociation laser intensity. It clearly shows that the $RbCs^+$ molecular ion intensity increases as PA laser intensity increases until the saturation effect appears. The curves in Fig. 4(b) are the fittings to the theoretical model by Bohn and Julienne for photoassociation in strong laser fields [52]. The model based on scattering theory yields a general analytic expression for the photoassociation rate:

$$|S|^2 = \gamma\Gamma/4(\gamma+\Gamma)^2 = II_S/4(I+I_S)^2, \tag{8}$$

where γ is the natural linewidth of the transition and Γ denotes the coupling strength defined by the overlap of the initial continuum wave function and the final bound-state wave function. I is the PA laser intensity, and the saturation intensity I_S is introduced according to $I/I_S = \Gamma/\gamma$. The saturation intensities for different rotational levels are obtained by fitting the measured experimental data with Eq. (8). Although we did not do a systematic study of line shapes, resonant broadening increases as expected. We do not observe the PA laser-induced frequency shift of RbCs molecules with our experimental accuracy.

C. Dipole moment measurement of (2) $^3\Pi$ state RbCs molecules

In order to determine the permanent EDM of (2) $^3\Pi$ state RbCs molecules, we measure the dc Stark spectroscopy on the transition frequencies between $J = 0, 1, 2$, components of this level and the continuum atom state. The measured Stark shifts of the lowest three rotational levels of the (2) $^3\Pi$ state are shown in Figs. 5(a) and 5(b) with static electric fields from 0 to 350 V/cm. The dye laser and PA laser intensities are 1.91 mJ/mm^2 and 120 W/cm^2, respectively.

As the initial state of the PA process is a pair of free atoms without a permanent EDM, every change in the position is exclusively due to the Stark effect of the excited level. The electric-field-induced shifts of rotational levels of the (2) $^3\Pi$ state at the weak-field regime can be written as [53]

$$\begin{aligned}\Delta W &= -\mu^2 E_s^2/6hB_v \quad (J=0)\\ &= \frac{\mu^2 E_s^2}{hB_v}\frac{J(J+1)-3m_J^2}{2J(J+1)(2J-1)(2J+3)} \quad (J\neq 0),\end{aligned} \tag{9}$$

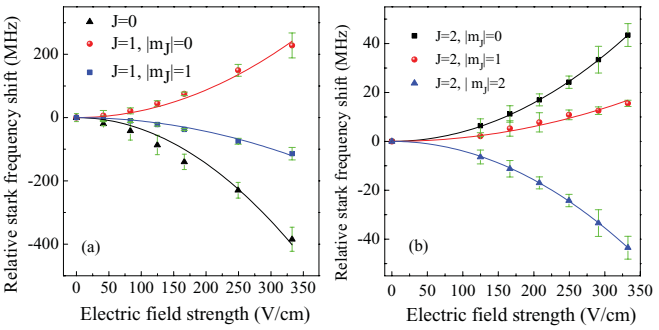

FIG. 5. (Color online) Stark effect of (2) $^3\Pi$ state RbCs molecules. Stark shifts of RbCs molecules for rotational number (a) $J = 0, 1$ and (b) $J = 2$ are shown vs dc electric fields from 0 to 350 V/cm. The error bars correspond to standard deviations in mean value, averaged over five repeated experimental measurements while keeping other parameters constant. All curves are fitted to a quadratic Stark effect, denoted by Eq. (9).

where μ is the EDM, E_s is static electric-field strength, and m_J is the projection of J onto the molecular axis. Fitting the experimental data with Eq. (9) and using the measured rotational constant $B_v = 0.01304$ cm^{-1}, we derive an average EDM $\mu = 4.7(6)$ D. The measured permanent dipole moment is a little larger than the theoretical value calculated by Lim *et al.* [54]. The difference arises mainly from the uncertainty on the electric-field strength. This large dipole moment allows the molecules to be polarized by moderate electric fields and will facilitate exploration of the interaction with the electric field [55].

The quadratic dependence of Stark shifts on the electric-field strength agrees well with theory in the weak-field regime. As the field strength increases, the deviation between measured Stark shift and theoretical fit value becomes larger. This is consistent with the theoretical prediction about the evolution of rovibrational state as electric-field strength increases [56]. Thus it is more accurate to determine the EDM at the weak-field regime. In addition, the full width at half maximum and intensity of photoassociative line shape also increase as the electric field increases.

IV. CONCLUSIONS

In conclusion, we have produced RbCs molecules in the (2) $^3\Pi$ state via photoassociation in a ^{85}Rb-^{133}Cs species dark spontaneous force optical trap. Some parts of the excited molecules spontaneously decay to the metastable ground state, which are ionized by resonance-enhanced two-photon ionization through the (3) $^3\Pi$ state and detected by a time-of-flight mass spectrometer. When the PA laser is tuned to the resonance frequency of RbCs molecules, a typical production rate in the metastable ground state, which contains different rovibrational levels, is estimated to be 2.5×10^4 s^{-1}. In addition to the appearing of $RbCs^+$ molecular ion, the Rb^+ and Cs^+ atomic ions and the $Cs_2{}^+$ molecular ion are also enhanced in the presence of the PA laser. The $RbCs^+$ molecular ion intensity is approximately linear with respect to the ionization laser intensity in the range of 0–0.76 mJ/mm^2, and saturation is observed as the ionization laser intensity increases up to about 1.53 mJ/mm^2. A rate equation for the photoionization process

is introduced to explain this relationship. The experimental results and theoretical fit agree well at large pulsed dye laser intensity. The reason for the imperfect fit at low dye laser intensity is that the transition from ground state to excited state is more likely to saturate than the transition from excited state to ionic state [51], resulting in the linear dependence. With the highly sensitive detection efficiency, we have observed the (2) $^3\Pi$ state RbCs molecules with rotational number up to $J = 4$. The rotational constant and centrifugal distortion constant based on the nonrigid model are measured to be 0.01304 and 0.000015 cm^{-1}, respectively. Considering standard deviations of experimental and theoretical values, the observed short-range state is assigned to the $v = 8$, (5)0^+ state. The much lower vibrational levels need to be explored further. The dependence of RbCs molecular ion intensity on PA laser intensity was investigated in the range of 0–140 W/cm^2, and saturation appears as we expected. The electric dipole moment of these (3) $^3\Pi$-state RbCs molecules at short range is measured to be about 4.7(6) D using the dc Stark effect in static electric fields, which is a little larger than the value calculated by Lim *et al.* [54]. This large electric dipole moment allows the molecules to be polarized by moderate electric fields and will facilitate exploration of the interaction with the electric field. The (2) $^3\Pi$ state at short range also provides a simple pathway to produce RbCs molecules in the lowest level of the $X\ ^1\Sigma^+$ ground state due to spin-orbit coupling between the (2) $^3\Pi$ and (2) $^1\Pi$ states. Inspired by the simple method, we will study the population of the singlet ground state and investigate the selective translation of rovibrational states via STIRAP in the future.

ACKNOWLEDGMENTS

The authors thank Dr. D. Sheng and Dr. X. L. Zhang for helpful discussions and Dr. L. J. Zhang for technique support. This work was supported by the National Basic Research Program of China (973 Program, Grant No. 2012CB921603), the Major Program of the National Natural Science Foundation of China (Grant No. 10934004), and the National Natural Science Foundation of China (Grants No. 60808009, No. 60978018, No. 60978001, No. 61008012, No. 11174187, and No. 11004125).

[1] L. D. Carr, D. DeMille, R. V. Krems, and J. Ye, New J. Phys. **11**, 055049 (2009).
[2] L. Santos, G. V. Shlyapnikov, P. Zoller, and M. Lewenstein, Phys. Rev. Lett. **85**, 1791 (2000).
[3] M. G. Kozlov and L. N. Labzowsky, J. Phys. B **28**, 1933 (1995).
[4] S. Ospelkaus, K.-K. Ni, D. Wang, M. H. G. de Miranda, B. Neyenhuis, G. Quéméner, P. S. Julienne, J. L. Bohn, D. S. Jin, and J. Ye, Science **327**, 853 (2010).
[5] D. DeMille, Phys. Rev. Lett. **88**, 067901 (2002).
[6] T. Köhler, K. Göral, and P. S. Julienne, Rev. Mod. Phys. **78**, 1311 (2006).
[7] K. M. Jones, E. Tiesinga, P. D. Lett, and P. S. Julienne, Rev. Mod. Phys. **78**, 483 (2006).
[8] J. Deiglmayr, A. Grochola, M. Repp, K. Mörtlbauer, C. Glück, J. Lange, O. Dulieu, R. Wester, and M. Weidemüller, Phys. Rev. Lett. **101**, 133004 (2008).
[9] C. Haimberger, J. Kleinert, M. Bhattacharya, and N. P. Bigelow, Phys. Rev. A **70**, 021402 (2004).
[10] D. Wang, J. Qi, M. F. Stone, O. Nikolayeva, H. Wang, B. Hattaway, S. D. Gensemer, P. L. Gould, E. E. Eyler, and W. C. Stwalley, Phys. Rev. Lett. **93**, 243005 (2004).
[11] J. M. Sage, S. Sainis, T. Bergeman, and D. DeMille, Phys. Rev. Lett. **94**, 203001 (2005).
[12] N. Nemitz, F. Baumer, F. Münchow, S. Tassy, and A. Görlitz, Phys. Rev. A **79**, 061403 (2009).
[13] A. Ridinger, S. Chaudhuri, T. Salez, D. R. Fernandes, N. Bouloufa, O. Dulieu, C. Salomon, and F. Chevy, Eur. Phys. Lett. **96**, 33001 (2011).
[14] C. A. Stan, M. W. Zwierlein, C. H. Schunck, S. M. F. Raupach, and W. Ketterle, Phys. Rev. Lett. **93**, 143001 (2004).
[15] E. Wille, F. M. Spiegelhalder, G. Kerner, D. Naik, A. Trenkwalder, G. Hendl, F. Schreck, R. Grimm, T. G. Tiecke, J. T. M. Walraven, S. J. J. M. F. Kokkelmans, E. Tiesinga, and P. S. Julienne, Phys. Rev. Lett. **100**, 053201 (2008).
[16] B. Deh, C. Marzok, C. Zimmermann, and Ph. W. Courteille, Phys. Rev. A **77**, 010701 (2008).
[17] E. Hodby, S. T. Thompson, C. A. Regal, M. Greiner, A. C. Wilson, D. S. Jin, E. A. Cornell, and C. E. Wieman, Phys. Rev. Lett. **94**, 120402 (2005).
[18] K. Pilch, A. D. Lange, A. Prantner, G. Kerner, F. Ferlaino, H.-C. Nägerl, and R. Grimm, Phys. Rev. A **79**, 042718 (2009).
[19] E. S. Shuman, J. F. Barry, and D. DeMille, Nature (London) **467**, 820 (2010).
[20] S. K. Tokunaga, W. Skomorowski, P. S. Żuchowski, R. Moszynski, J. M. Hutson, E. A. Hinds, and M. R. Tarbutt, Eur. Phs. J. D **65**, 141 (2011).
[21] K.-K. Ni, S. Ospelkaus, M. H. G. de Miranda, A. Péer, B. Neyenhuis, J. J. Zirbel, S. Kotochigova, P. S. Julienne, D. S. Jin, and J. Ye, Science **322**, 231 (2008).
[22] S. Ospelkaus, A. Péer, K.-K. Ni, J. J. Zirbel, B. Neyenhuis, S. Kotochigova, P. S. Julienne, J. Ye, and D. S. Jin, Nat. Phys. **4**, 622 (2008).
[23] K. Aikawa, D. Akamatsu, M. Hayashi, K. Oasa, J. Kobayashi, P. Naidon, T. Kishimoto, M. Ueda, and S. Inouye, Phys. Rev. Lett. **105**, 203001 (2010).
[24] H. Wang and W. C. Stwalley, J. Chem. Phys. **108**, 5767 (1998).
[25] P. S. Żuchowski and J. M. Hutson, Phys. Rev. A **81**, 060703 (2010).
[26] M. H. Anderson, J. R. Ensher, M. R. Matthews, C. E. Wieman, and E. A. Cornell, Science **269**, 198 (1995).
[27] T. Weber, J. Herbig, M. Mark, H.-C. Nägerl, and R. Grimm, Science **299**, 232 (2003).
[28] D. J. McCarron, H. W. Cho, D. L. Jenkin, M. P. Köppinger, and S. L. Cornish, Phys. Rev. A **84**, 011603 (2011).
[29] A. D. Lercher, T. Takekoshi, M. Debatin, B. Schuster, R. Rameshan, F. Ferlaino, R. Grimm, and H.-C. Nägerl, Eur. Phys. J. D **65**, 3 (2011).

[30] K. Pilch, A. D. Lange, A. Prantner, G. Kerner, F. Ferlaino, H.-C. Nägerl, and R. Grimm, Phys. Rev. A **79**, 042718 (2009).
[31] M. Debatin, T. Takekoshi, R. Rameshan, L. Reichsöllner, F. Ferlaino, R. Grimm, R. Vexiau, N. Bouloufa, O. Dulieu, and H.-C. Nägerl, Phys. Chem. Chem. Phys. **13**, 18926 (2011).
[32] H. W. Cho, D. J. McCarron, D. L. Jenkin, M. P. Köppinger, and S. L. Cornish, Eur. Phys. J. D **65**, 125 (2011).
[33] W. C. Stwalley, J. Banerjee, M. Belos, R. Carollo, M. Recore, and M. Mastroianni, J. Phys. Chem. A **114**, 81 (2010).
[34] B. E. Londoño, J. E. Mahecha, E. Luc-Koenig, and A. Crubellier, Phys. Rev. A **80**, 032511 (2009).
[35] C. Gabbanini and O. Dulieu, Phys. Chem. Chem. Phys. **13**, 18905 (2011).
[36] A. R. Allouche, M. Korek, K. Fakherddin, A. Chaalan, M. Dagher, F. Taher, and M. Aubert-Frécon, J. Phys. B **33**, 2307 (2000).
[37] H. Fahs, A. R. Alloche, M. Korek, and M. Aubert-Frcon, J. Phys. B **35**, 1501 (2002).
[38] Z. H. Ji, H. S. Zhang, J. Z. Wu, J. P. Yuan, Y. T. Zhao, J. Ma, L. R. Wang, L. T. Xiao, and S. T. Jia, Chin. Phys. Lett. **28**, 083701 (2011).
[39] J. Deiglmayr, P. Pellegrini, A. Grochola, M. Repp, R. Côté, O. Dulieu, R. Wester, and M. Weidemüller, New J. Phys. **11**, 055034 (2009).
[40] C. G. Townsend, N. H. Edwards, K. P. Zetie, C. J. Cooper, J. Rink, and C. J. Foot, Phys. Rev. A **53**, 1702 (1996).
[41] M. H. Anderson, W. Petrich, J. R. Ensher, and E. A. Cornell, Phys. Rev. A **50**, 3597 (1994).
[42] W. Ketterle, K. B. Davis, M. A. Joffe, A. Martin, and D. E. Pritchard, Phys. Rev. Lett. **70**, 2253 (1993).
[43] C. Gabbanini, A. Fioretti, A. Lucchesini, S. Gozzini, and M. Mazzoni, Phys. Rev. Lett. **84**, 2814 (2000).
[44] T. Takekoshi, B. M. Patterson, and R. J. Knize, Phys. Rev. A **59**, 5 (1999).
[45] A. Fioretti, D. Comparat, A. Crubellier, O. Dulieu, F. Masnou-Seeuws, and P. Pillet, Phys. Rev. Lett. **80**, 4402 (1998).
[46] J. M. Hutson, J. Phys. B **14**, 851 (1981).
[47] P. Rambo, J. Schwarz, and J.-C. Diels, J. Opt. A **3**, 146 (2001).
[48] A. R. L. Caires, V. A. Nascimento, D. C. J. Rezende, V. S. Bagnato, and L. G. Marcassa, Phys. Rev. A **71**, 043403 (2005).
[49] M. W. Mancini, G. D. Telles, A. R. L. Caires, V. S. Bagnato, and L. G. Marcassa, Phys. Rev. Lett. **92**, 133203 (2004).
[50] C. Drag, B. L. Tolra, O. Dulieu, D. Comparat, M. Vatasescu, S. Boussen, S. Guibal, A. Crubellier, and P. Pillet, IEEE J. Quantum Electron. **36**, 1378 (2000).
[51] C. Haimberger, J. Kleinert, O. Dulieu, and N. P. Bigelow, J. Phys. B **39**, S957 (2006).
[52] J. L. Bohn and P. S. Julienne, Phys. Rev. A **60**, 414 (1999).
[53] M. Peter and M. W. P. Strandberg, J. Chem. Phys. **26**, 1657 (1957).
[54] I. S. Lim, W. C. Lee, Y. S. Lee, and G.-H. Jeung, J. Chem. Phys. **124**, 234307 (2006).
[55] R. González-Férez, M. Mayle, P. Sánchez-Moreno, and P. Schemelcher, Europhys. Lett. **83**, 43001 (2008).
[56] R. González-Fárez, M. Mayle, and P. Schemelcher, Chem. Phys. **329**, 203 (2006).